TURBOMACHINERY & PUMP SYMPOSIA | VIRTUAL
DECEMBER 8-10, 2020
SHORT COURSES: DECEMBER 7, 2020

INFLUENCE OF THE SHAPE OF THE IMPELLER BLADE TRAILING EDGE ON SINGLE AND TWO-PHASE AIR-WATER FLOWS IN A CENTRIFUGAL PUMP

Michael Mansour
Graduate Research Assistant
Laboratory of Fluid Dynamics & Technical Flows
University of Magdeburg "Otto von Guericke"
Magdeburg, 39106, Germany

Trupen Parikh
Graduate Research Assistant
Laboratory of Fluid Dynamics & Technical Flows
University of Magdeburg "Otto von Guericke"
Magdeburg, 39106, Germany

Dominique Thévenin
Faculty Dean and Chair Professor
Faculty of Process Engineering
Laboratory of Fluid Dynamics & Technical Flows
University of Magdeburg "Otto von Guericke"
Magdeburg, 39106, Germany

Michael Mansour is currently working as a research assistant at the chair of Fluid Dynamics and Technical Flows at the University of Magdeburg, Germany. He is funded by the research project "Liquid-gas transport by centrifugal pumps". He received his B.S. and M.S. degrees in Mechanical Engineering from Helwan University in Cairo, Egypt. From 2009 to 2014, he worked at Helwan University as a research and teaching assistant. Afterward, he received a partial Ph.D. scholarship from the Egyptian Government together with the German KAAD ideal sponsorship to support his Ph.D. in Germany. He has finished his Ph.D. degree in January 2020 under the supervision of Prof. Dominique Thévenin. Michael's research includes modern optical measurements for gas-liquid two-phase flows in centrifugal pumps and numerical simulations of two-phase flows in pumps, pipes, and several other flow channels. Additionally, he has several research papers concerning flow mixing and heat transfer in helical pipes.

Trupen Parikh completed his B.E. in Mechanical engineering at NMAMIT, Nitte, India. In 2014, he went on to work as a Junior Mechanical engineer in India for a year. Later, he joined as a master student in Chemical and Energy Engineering at the Otto von Guericke University Magdeburg. He has recently completed his Master's study under the supervision of the Ph.D. candidate Michael Mansour and Prof. Dominique Thévenin at the Laboratory of Fluid Dynamics & Technical Flows at the Otto von Guericke University Magdeburg, Germany. He worked as a Research Assistant in the same department focusing on experimental pump investigation. His thesis and research area mainly focus on numerical analysis of two-phase gas/liquid flows in turbomachinery.

Dominique Thévenin is currently the Dean of the Faculty of Process Engineering at the Otto von Guericke University Magdeburg. Since 2002, he holds the Chair of the Laboratory of Fluid Dynamics and Technical Flows, including teaching and research. Prof. Thévenin started his scientific career in 1989 after completing his studies at École Polytechnique, France. Subsequently, in 1992, he received his Ph.D. degree in energy technology at the Ecole Centrale Paris, France. His research interests involve in particular Direct Numerical Simulation (DNS) applied to multiphase flows, reactive flows, sprays, laminar and turbulent flames. But he also considers medical flows, CFD-based optimization of turbomachines, as well as mixing and separation processes.

Copyright© 2019 by Turbomachinery Laboratory, Texas A&M Engineering Experiment Station

ABSTRACT

In this study, the performance of a radial-type centrifugal pump was investigated for different single and two-phase flow conditions to evaluate the influence of the shape of the impeller blade trailing edge. For that purpose, two geometrically similar semi-open impellers with two common blade trailing edge profiles were manufactured and experimentally compared, considering a round trailing edge (RTE) and a trimmed trailing edge (TTE). The impellers and pump casing were made of transparent acrylic glass to allow visualization and recording of the two-phase flow regimes by a high-speed camera. Additionally, 3D URANS numerical single-phase simulations were performed for the whole pump geometry to understand the performance changes between the two impeller designs. The standard moving-mesh approach combined with the $k - \omega$ SST turbulence model was used to simulate the pump flow. In the experiments, the hysteresis effects were studied by incorporating two different procedures to set the desired operating conditions. The pump performance was measured and analyzed for both constant gas volume fractions and constant air flow rates at the pump inlet. The results show that the pump with TTE impeller has considerably lower performance compared to the RTE impeller for single-phase as well as most of the two-phase flow conditions. The reason for this lower performance could be revealed by the numerical simulations, where the interaction between the TTE impeller and the volute tongue led to a bigger separation. Furthermore, the experiments show that the TTE impeller has a much larger surging region compared to the RTE impeller. The reason is that the TTE impeller is more prone to gas accumulation within blade channels at lower gas volume fractions due to its lower performance. This limits its working range further, particularly at 5 % gas volume fraction. Comparing different experimental procedures, hysteresis effects were observed for the RTE impeller only for gas volume fractions between 4 and 5 %, while the TTE impeller has increased hysteresis effects for gas volume fractions between 3 and 5 %. Finally, two-phase flow regime maps were generated and associated with the pump performance. Based on the results shown in this study, the round trailing edge is always recommended to ensure higher single and two-phase performances, lower gas accumulations, and more limited surging and performance hysteresis.

INTRODUCTION

The usage of centrifugal pumps to transport single and two-phase air-water flows is very relevant for numerous industrial and engineering applications. Primarily, designed to handle single-phase mixtures, many industrial applications now require the same flexibility, broad applicability, and similar performance for two-phase flow conditions as well. However, while transporting two-phase mixtures, the pump performance remarkably drops even at low gas volume fractions of about 1 %. The performance reduction occurs due to the presence of gas accumulation within the impeller channels, which increases as the gas volume fraction is increased [1–7]. The fundamental reason for this performance degradation being the inability of the pump impeller to efficiently transfer the momentum energy to the two-phase mixture. This problem is of much concern in various applications, such as petroleum and natural gas production [1,8], agriculture [7], geothermal power plants [9], refrigeration systems [10], nuclear power plants [4,11,12], chemical processes, paper industry, and wastewater treatment [13]. This has motivated a large field of research to explore various pump designs and capabilities to better handle and transport two-phase mixtures with minimum performance deterioration and a wider working range.

Pump operating under two-phase flow conditions can undergo a series of problems when the gas volume fraction at the pump inlet is increased. This starts with typical pump performance deterioration at low gas volume fraction between 1 % and 3 %. With further increase in the gas volume fraction, the gas starts to accumulate within the impeller channel starting in most cases from the blade leading edge, radially growing outwards with the increase of the gas contents, leading to huge pockets on all blades. This phenomenon is commonly known as “gas locking” [1–6]. Additionally, a severe phenomenon called “pump surging” can occur. During this condition, rapid and unstable accumulation and discharge of big gas pockets can occur, which leads to strong vibrations and obvious flow instabilities accompanied by fluctuations in all pump parameters, including for example pump head and flow rate [5,14–19]. Furthermore, as the gas volume fraction is increased to values around 7 % to 10 % in part-load conditions (flow rates lower than the design flow), the pump can completely stop generating any head, which is known as “pump breakdown”[3–5,13,14].

Several experimental investigations have been performed using various visualizing techniques to study the complex two-phase flow patterns and the corresponding flow behavior that affect the pump performance [5,20,21]. Accordingly, the two-phase flow patterns were classified into bubbly flow (dispersed spherical bubbles) at low gas volume fractions, agglomerated bubble flow (bubble coalescence together forming agglomerated ones) at low to medium gas volume fractions, alternating pocket flow (gas pockets appear alternatively on blade suction and/or pressure side) at medium to high gas volume fractions and segregated flow (separated flow due to large gas accumulation within impeller channels) at very high gas volume fractions [5,14,15,17,20,22].

The presence of large separations in the flow was found to be the main reason for the development of huge gas accumulations in two-phase flows [14], due to the low-pressure available in the separation zone. Such low-pressure zones can mainly occur in pumps near the blade suction and/or pressure sides or near the volute tongue [7,23–28]. Several studies have shown that increasing the turbulence levels can help to disturb these gas accumulations and further enhance mixing between the two phases, boosting the pump performance [14,27]. These have been done by various methods like increasing the impeller blade tip clearance gap [5,27], placing an inducer upstream of the impeller [5,27], increasing the rotational speeds [14,17,19,29], introducing surfactant within the two-phase flow [8].

Copyright© 2020 by Turbomachinery Laboratory, Texas A&M Engineering Experiment Station

The profiles of the leading and trailing edges of the impeller blade are also very important parameters concerning the pump and the cavitation performance. Changing the leading edge profile can only slightly affect the pump head, yet it can strongly affect the cavitation performance [30–32]. On the other hand, the profile of the trailing edge is very influential concerning the pump head since it is directly related to the distance between the blades and the flow deceleration near the impeller outlet [33]. Additionally, the trailing edge profile impacts the generated vortex shedding behind it, which changes the flow behavior in the volute and modifies the complex interaction between the impeller blades and the volute tongue [34–37].

For instance, Gao el. al [34] investigated the influence of five different blade trailing edges on the performance and the pressure pulsations in a centrifugal pump. It was found that the round (circle) and the ellipse trailing edges have higher pump performance (head and efficiency) compared to the trimmed (original) trailing edge. Kye et. al [28] used large eddy simulation to numerically simulate the centrifugal pump and showed that vortex shedding from the blade trailing edge can cause stronger vortices in a wider region inside the volute. The attempts done in the literature to improve the pump performance by modifying the trailing edge considered also recently complex profiles, i.e. V-cut [38] and sinusoidal [37] profiles. Warda et al. [38] compared seven different blade trailing edges and proposed that a V-cut blade trailing edge comparatively provides better efficiency than all other designs at high rotational speeds (6000 rpm). Furthermore, it was shown that the effects of blade trailing edge become even higher at higher rotational speeds.

Although several interesting results could be obtained in the literature, the previous investigations concerning the influence of the trailing edge profile were only limited to single-phase flow. Thus, the main objective of the present work is to compare two typical types of blade trailing edges, i.e. round trailing edge (RTE) and trimmed trailing edge (TTE), also for two-phase air-water flow in a centrifugal pump. The impellers and the pump casing were made of transparent acrylic glass to allow full visualization and recording of the two-phase flow regimes by a high-speed camera. The pump performance was measured and analyzed for both constant gas volume fractions and constant air flow rates at the pump inlet. The comparisons cover also the performance deterioration, the flow instabilities, and the performance hysteresis by applying two different procedures to set the desired operating conditions [5,6]. Additionally, sample single-phase simulations have been done using the moving-mesh approach and the $k-\omega$ SST turbulence model to explain the internal flow details, complementing the experimental observations. The present analysis provides detailed insights into the pumping performance of these two blade trailing edges for a variety of two-phase flow conditions.

EXPERIMENTAL TEST-RIG

A view of the pump casing, the two impellers, and the whole loop of the experiments are shown in Figure 1a, 1b, and 1c, respectively. As mentioned in the introduction, the whole pump casing and the two impellers were made entirely from transparent glass to allow complete flow visualization. Additionally, the impellers were designed with 6 cylindrical (non-twisted) blades to maximize the flow visualization. The two-phase flow patterns were recorded by using a high-speed camera with 2016 x 2016 pixels resolution. To illuminate the flow inside the pump, 4 LED lamps were distributed around the pump casing as shown in Figure 1a. In this way, the interface between air and water can be observed. The window where the two-phase flow patterns were observed are indicated by dashed rectangles in Figure 1a. The (semi-open) impeller is installed with a standard tip-clearance gap ($S\ /b_2 = 2.5$ %), where b_1 and b_2 are the impeller blade inlet and outlet widths. Figure 1b shows the two impellers with either a round trailing edge (RTE) or a trimmed trailing edge (TTE), while all other geometrical parameters are kept identical. The diameter of the round trailing edge is equal to the blade thickness.

As shown in Figure 1c, the suction pipe of the pump is connected to a water tank with a total volume of 6.3 m^3 to provide a closed-loop operation. The flow rates of both phases are measured separately before being mixed. The water flow rate (Q_w) is measured by an electromagnetic flow meter (with ± 0.5 % RD accuracy) and adjusted by a motorized gate valve positioned on the discharge line. The air mass flow rate ($\dot{m}_a$) is measured by a mass-flow meter (with ± 0.5 % RD plus ± 0.1 % FS accuracy) and regulated by a throttle valve. The air flow is then mixed with the water phase before entering the pump at the center of the inlet pipe via a gas distribution nozzle as indicated in Figure 1c. The pressure before (P_1) and after (P_2) the pump is measured by two absolute pressure sensors (with ± 0.25 % FS accuracy). The flow temperature (T) is monitored by a temperature sensor (with ± 0.3 K maximum absolute error) installed near the air injection. The suction conditions (P_1 and T) are used to determine the inlet air volume flow rate (Q_a) and the inlet air volume fraction (ε). The suction pressure (P_1) was always bounded between 1.28 and 1.14 bar in the experiments, corresponding to the minimum and the maximum flow rates, respectively.

The pump is driven by a variable speed motor (5.7 kW, with 3000 rpm maximum rotational speed), where the rotational speed (n) is measured by an analog tachometer (with 1 % RD accuracy). A torque sensor (with ± 0.4 % FS accuracy) is installed on the motor shaft to measure the shaft torque (τ) and obtain the pump efficiency (η). Since the pump components are made of acrylic glass, a low rotational speed of $n = 650$ rpm was kept for the present investigations to prevent strong vibrations that occur at higher speeds, which can be destructive for the pump parts. In this case, the specific speed of the pump is approximately $n_q = 21$ ($n_s = 1084$) min^{-1}. Further details regarding the test-rig and the impeller dimensions can be found in our previous publications [5,14,27].

Copyright© 2020 by Turbomachinery Laboratory, Texas A&M Engineering Experiment Station

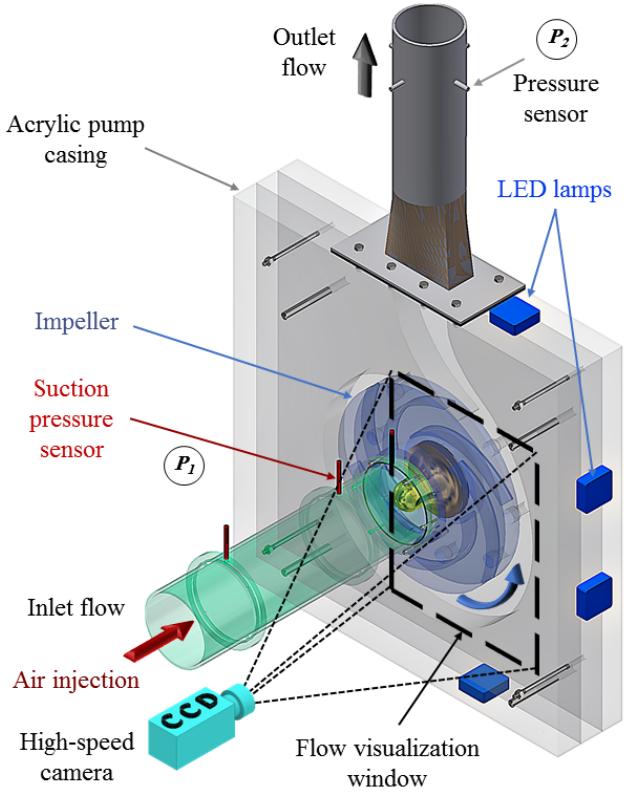

a) 3D view of the pump casing.

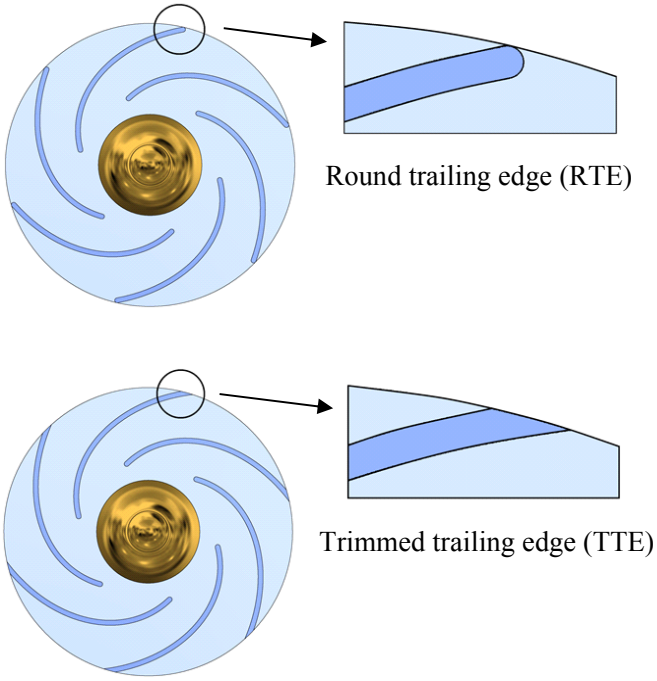

b) Details of the considered trailing edges.

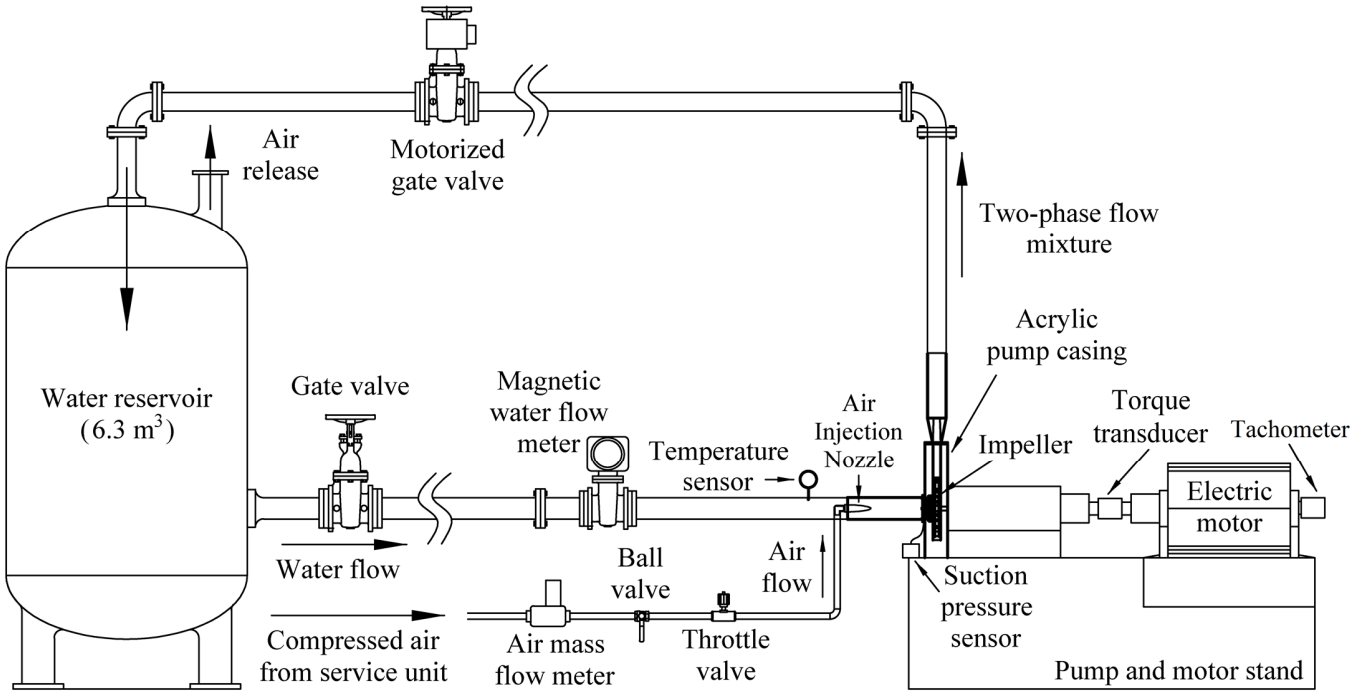

c) Schematic sketch of the experimental loop.

Figure 1. Details of the experimental test-rig.

Copyright© 2020 by Turbomachinery Laboratory, Texas A&M Engineering Experiment Station

NUMERICAL MODELING

Simulation domain and grid

The details of the simulation domain are shown in Figure 2a. As shown, the simulation domain consists of 3 different parts connected via in-place interfaces, which are the inlet pipe, the rotating zone (around the impeller), and (3) the volute with the outlet pipe. The length-to-diameter ratios of the inlet and outlet pipes are approximately 4 and 5, respectively. The pressure is monitored in the simulations in corresponding locations as the experiments.

The grid used in the present simulations has been adopted from our previous study [27], after performing a grid independence test. A polyhedral grid was generated for the entire domain with additional refinement within the rotating zone to ensure precise capturing of the flow within the pump impeller. 8 prism layers were created along all walls to accurately resolve the flow in the boundary layer. The first layer thickness was kept sufficiently small to keep the average dimensionless wall distance y^+ always below 1. A view of the final grid is shown in Figure 2b with a total of 5.11 million cells. Additional details and grid independence data can be found in [27].

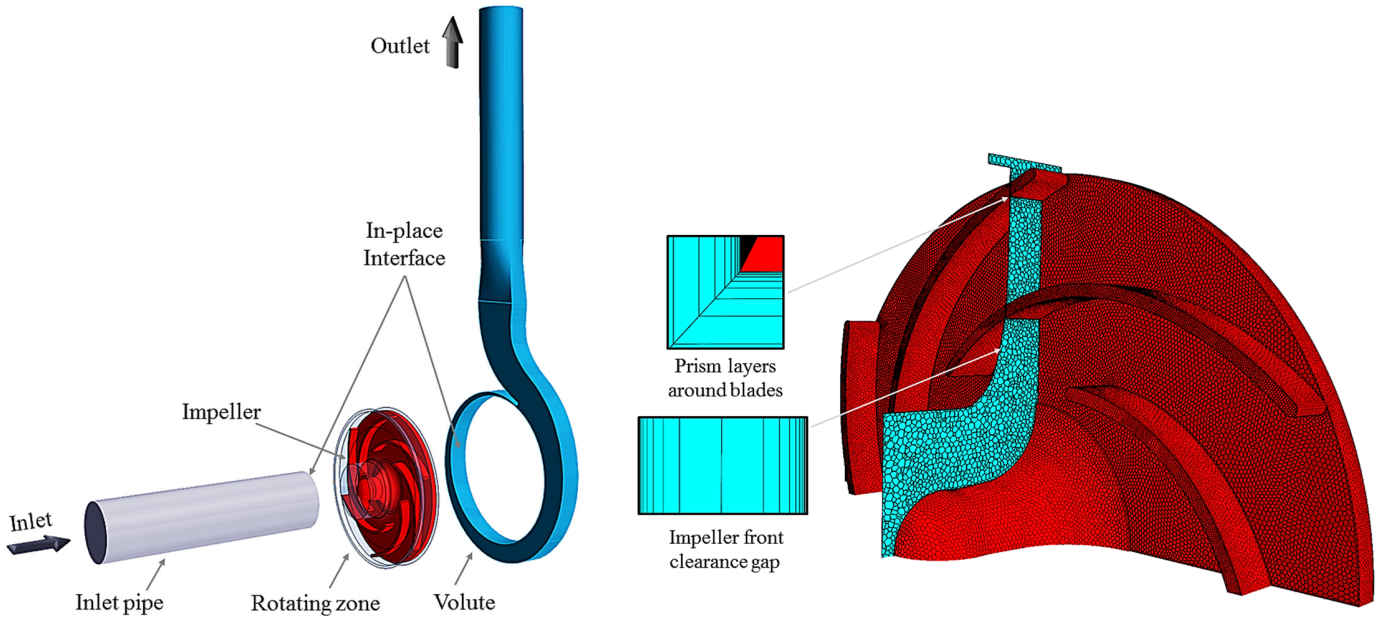

a) Simulation domain. b) Numerical grid.

Figure 2: Details of the simulation domain and the numerical grid.

Model description

3D URANS single-phase simulations were performed to provide internal flow details, in particular the interaction between the impeller blades and the volute tongue. The $k-\omega$ shear stress transport (SST) model [39] was employed for turbulence modeling. This model has been widely used for modeling flow in pumps since it can accurately capture strong pressure gradients and flow separations within the flow [27,40–44]. A rigid body motion (moving mesh) technique was used to model the transient impeller rotation. A second-order upwind scheme was applied together with a segregated solver. The continuity and momentum equations are given by Equations (1) and (2), respectively.

$$\frac{\partial \rho}{\partial t} + \nabla \cdot \left(\rho \vec{V}\right) = 0 \tag{1}$$

$$\rho \frac{D\vec{V}}{Dt} = \rho \vec{g} - \vec{\nabla} \cdot p + \mu \vec{\nabla}^2 \cdot \vec{V} \tag{2}$$

where ρ is the fluid density, $\vec{V}$ is the flow velocity, $\vec{g}$ is the gravitational acceleration, p is the pressure, and μ is the dynamic viscosity. Further details can be found in [45]. Water with a density of $\rho = 997.56$ kg/m^3 and a dynamic viscosity of $\mu = 8.887 \times 10^{-4}$ Pa·s.

Copyright© 2020 by Turbomachinery Laboratory, Texas A&M Engineering Experiment Station

The time-step was selected after performing a timestep study using three different timesteps in [27]. Finally, a timestep of 1˚ was chosen, ensuring negligible changes in all pump parameters. For the applied timestep, the CFL (Courant–Friedrichs–Lewy) number is always below 1 for all simulations. 25 inner iterations were used to ensure enough convergence for each timestep by a drop of approximately three magnitudes of the residuals. The physical time of the simulation was kept 0.5 seconds, which corresponds to more than 5 impeller rotations. All the numerical results were averaged over 1 entire impeller rotations to get stable averaged values. Additional information concerning the time step independence study can be found in [27].

RESULTS AND DISCUSSION

In the present work, the pump performance is calculated in terms of the specific delivery work (Υ), which represents the total pump power per mass flow rate as defined by Equation (3), assuming an isothermal compression process for the air phase within the pump. In Equation (3), $\dot{\mu}$ is the air mass fraction, ρ_w is the water density, P_1 is the suction pressure, P_2 is the discharge pressure, R is the gas constant of air, T is the flow temperature, V_1 is the suction superficial flow velocity, V_2 is the discharge superficial flow velocity, z_1 is the suction elevation and z_2 is the discharge elevation. The air mass fraction ($\dot{\mu}$) is defined by Equation (4), where $\dot{m}_a$ and $\dot{m}_w$ are the mass flowrates of air and water, respectively and ρ_a is the air density. The superficial velocities in the suction and the delivery pipes (V_1 and V_2) are calculated from Equation (5) and (6), respectively, based on the continuity balance, where A_1 and A_2 are the suction and the discharge areas, respectively. The complete derivation of Equation (3) can be found in our previous study [5]. The performance of the pump was obtained for different gas volume fractions ε, which is defined by Equation (*7*), representing the fraction of the air volume flow rate to the total volume flow rate (Q_t). Here, Q_t is the sum of Q_a and Q_w, which are the air and water volume flowrates, respectively. Lastly, the shaft power (P_{Sh}) and the efficiency (η) are calculated by Equations (8) and (9), respectively.

$$\Upsilon = \frac{1-\dot{\mu}}{\rho_w}(P_2 - P_1) + \dot{\mu}\, R\, T \ln\left(\frac{P_2}{P_1}\right) + \frac{1}{2}(V_2^2 - V_1^2) + g(z_2 - z_1) \tag{3}$$

$$\dot{\mu} = \frac{\dot{m}_a}{\dot{m}_a + \dot{m}_w} = \frac{\rho_a\, Q_a}{\rho_a\, Q_a + \rho_w\, Q_w} \tag{4}$$

$$V_1 = \frac{Q_t}{A_1} \tag{5}$$

$$V_2 = \frac{Q_t}{A_2} \tag{6}$$

$$\varepsilon = \frac{Q_a}{Q_t} = \frac{Q_a}{Q_a + Q_w} \tag{7}$$

$$P_{Sh} = \tau \cdot 2\pi n/60 \tag{8}$$

$$\eta = \frac{\dot{m}\,\Upsilon}{P_{Sh}} \tag{9}$$

Single-phase flow performance

The experimental and the numerical single-phase performance curves, i.e. the normalized specific delivery work (Υ/Υ_{opt}), the efficiency (η), and the normalized shaft power ($P_{Sh}/P_{Sh\,opt}$) of the two impellers are compared in Figure 3a, b, and c, respectively. Here, the conditions corresponding to the best efficiency point (optimal conditions, Q_{opt}, Υ_{opt}, and $P_{Sh\,opt}$) of the RTE impeller is used for normalization in all figures. As can be seen, the performance of the RTE impeller is always higher than the TTE impeller along the entire working flow range. This is particularly evident at overload conditions where the normalized specific delivery work of the TTE impeller drops by about 29 % compared to the RTE impeller while at part-load conditions the drop is approximately 7.5 %. Concerning the efficiency, only limited changes can be seen between the two impellers at part-load conditions. However, at overload conditions, the efficiency of the TTE impeller is obviously lower than that of the RTE impeller. Accordingly, when the TTE impeller is used, the peak point of the efficiency is slightly shifted to a lower volume flow rate compared to the RTE impeller, thereby narrowing the effective working flow range of the pump. For the RTE profile, the distance between the blades is increased near the impeller outlet compared to the TTE (non-profiled). In this case, the flow is more effectively decelerated at the impeller outlet, increasing the pump head. Additionally, the interaction between the impeller blades and the volute tongue is improved in the case of RTE, leading to higher performance as will be illustrated by the simulations. Comparing the experimental and numerical curves in Figure 3, it can be seen that the simulations can commonly predict the trends of all pump parameters.

Copyright© 2020 by Turbomachinery Laboratory, Texas A&M Engineering Experiment Station

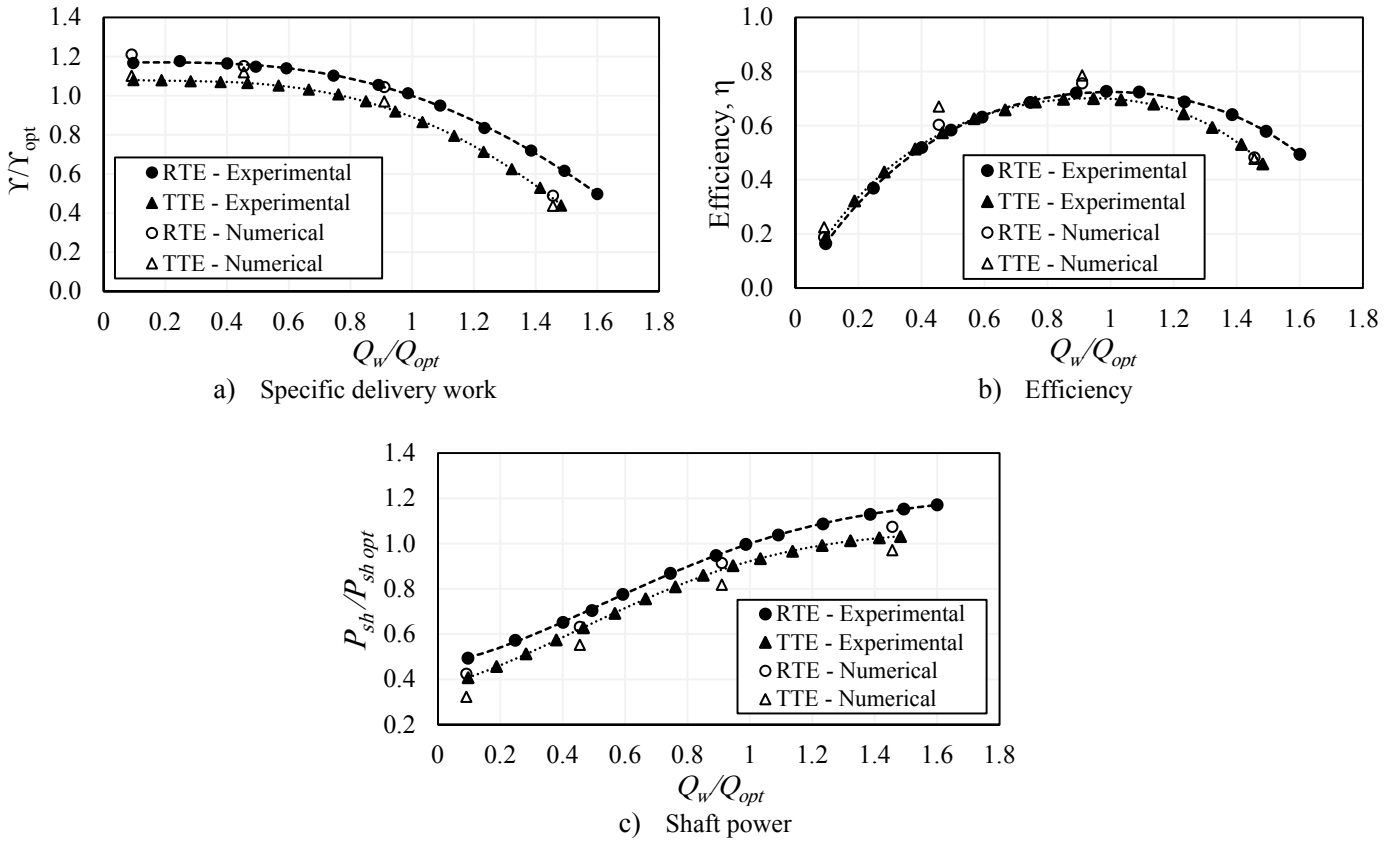

Figure 3: Comparison of single-phase performance for the round trailing edge (RTE) and the trimmed trailing edge (TTE) impellers.

Single-phase flow Visualization

Vorticity visualization from the numerical simulations in the two impellers and the blade trailing edge and volute tongue interaction are compared for both the impellers in Figure 4. The first and second rows represent the vorticity contours for the RTE and TTE impeller at part-load (Q_w/Q_{opt} = 0.1), optimal (Q_w/Q_{opt} = 1), and overload (Q_w/Q_{opt} = 1.6) conditions, respectively. It can be clearly noticed that as the flow is increased from part-load to overload conditions, flow separation near the volute tongue significantly increases for both impellers. However, the TTE impeller tends to show more vortices near the volute tongue. Additionally, the blade trailing edge vortex shedding (just behind the trailing edge) is the least at optimal conditions due to a more streamlined flow along the impeller blades, while, the blade vortex shedding is obviously higher at part-load and overload conditions. Concerning the vortex shedding for the TTE impeller at part-load conditions, the vortices tend to be directed within the impeller channels, limiting the head generated. Conversely, the RTE impeller can direct the flow better along the impeller exit, minimizing the vortices. Note that for the round trailing edge, the distance between the blades is increased near the impeller outlet compared to the trimmed trailing edge. In this case, the flow is more effectively decelerated at the impeller outlet, resulting in a higher pump head.

Now to compare the interactions between the blades and the volute tongue as well as the flow separation at the tongue, Figure 5 shows the 3D vortex structures via Q-criterion visualization at the optimal flow, i.e. Q_w/Q_{opt} = 1. The Q-criterion is a three-dimensional, scalar indicator that can be used to visualize the vortices and the wakes as spatial regions [46]. A value of Q-criterion = 20000 (1/s) was found suitable to differentiate the 3D vortex structures between the two considered impellers. Figure 5 confirms that the TTE impeller has a much bigger separation on the tongue, which is one of the main reasons for the reduced pump performance for this impeller.

Copyright© 2020 by Turbomachinery Laboratory, Texas A&M Engineering Experiment Station

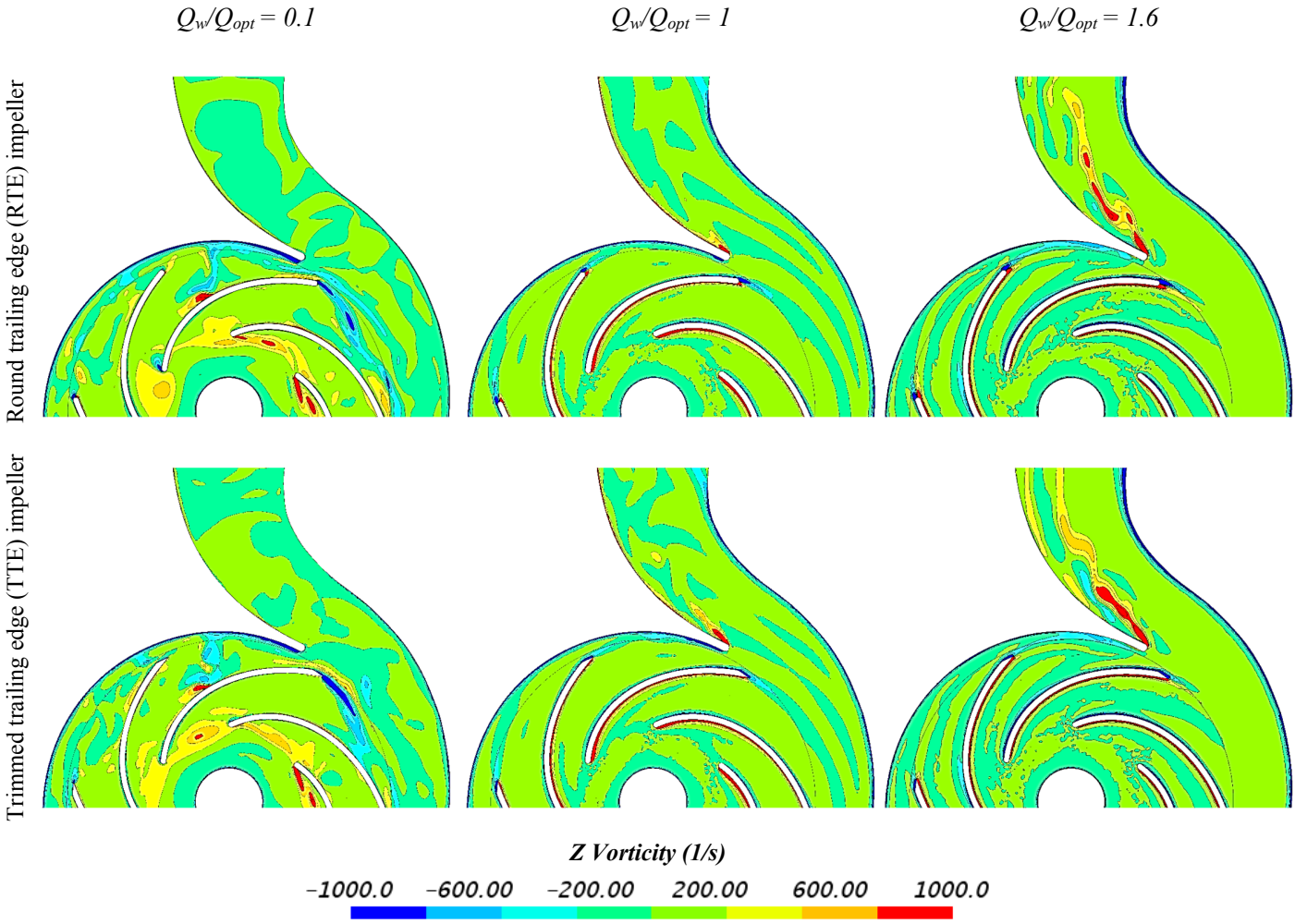

Figure 4: Vorticity visualization for the round trailing edge (RTE) and the trimmed trailing edge (TTE) impellers.

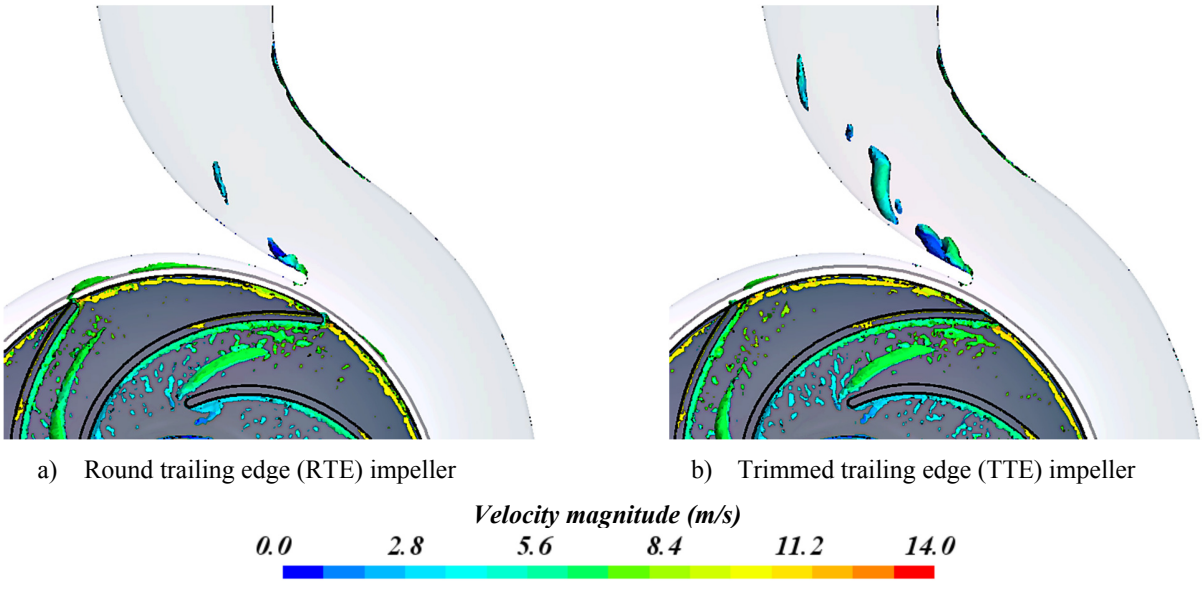

a) Round trailing edge (RTE) impeller

b) Trimmed trailing edge (TTE) impeller

Figure 5: Q-criterion visualization at optimal flow rate (Q_w/Q_{opt} = 1).

Copyright© 2020 by Turbomachinery Laboratory, Texas A&M Engineering Experiment Station

Two-phase flow performance

Performance curves of the round trailing edge (RTE) impeller

The normalized specific delivery work (Y/Y_{opt}) of the RTE impeller under two-phase flow conditions is shown in Figure 6. The results obtained by two different experimental procedures are shown simultaneously, i.e. an increasing approach starting from the minimum flow to the maximum flow and a decreasing approach starting from the maximum flow to the minimum flow [5,6]. This was done to examine possible hysteresis effects in the pump performance. The hysteresis is defined as the dependence of the pump performance on the history of reaching the desired conditions (the flow rates of air and water). Under two-phase pumping, obvious performance changes can appear for identical operating conditions, if the air flow is either reduced starting from an originally high value or increased starting from zero. Reducing the air flow from an originally high flow can allow prior accumulations of large air in the impeller, which can persist along the blades for some flow conditions, even after reducing the air flow rate to lower values, where smaller or even no pockets at all should appear when the air flow is increased from a zero value [5,6,14].

In Figure 6, the black-filled symbols and the dotted trend lines represent the results obtained by the increasing (first) procedure, while the empty symbols and the dashed trend lines donate the results recorded by the decreasing (second) procedure. Additionally, gray-filled symbols indicate the occurrence of strong flow instabilities (pump surging). The data points obtained by the two procedures are at some conditions clearly different, where a noticeable hysteresis can be seen, particularly at ε = 4 % and ε = 5 % at overload operations.

All negative pump phenomena including pump breakdown, surging, and cavitation are also highlighted in Figure 6. The pump completely loses its ability to transport the fluid in the breakdown region. Surging indicates the occurrence of strong system vibrations and large instabilities in the pump delivery, which can be observed near the maximum flow for ε = 4 % and ε = 5 %. Cavitation occurs only near the maximum flow rate of single-phase conditions, which is quickly damped as soon as a very small amount of air enters the pump [5,6,47,48]. As shown in Figure 6, by increasing the percentage of entrained air in the flow mixture, the specific delivery work of the pump (Y) is continuously reduced, and the performance curves get narrower. Up to ε = 3 %, the pump parameters are only very slightly reduced, showing minimal performance degradation. However, starting from ε = 4 % the performance is strongly decreased due to the beginning of big accumulations in the impeller, followed by several discontinuities in the pump performance till ε = 6 %.

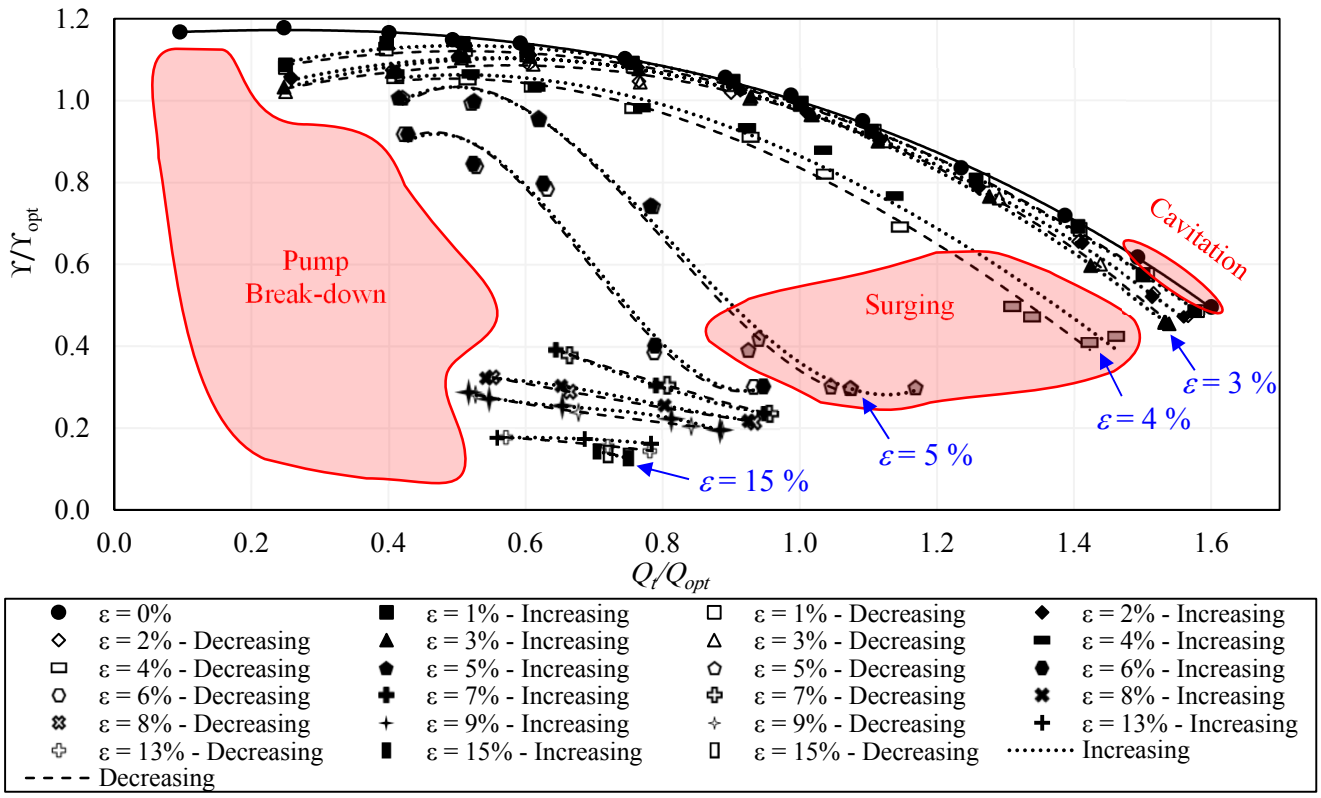

Figure 6: Normalized specific delivery work of the round trailing edge (RTE) impeller recorded by the first procedure (filled symbols and dotted curves) and the second procedure (empty symbols and dashed curves).

Copyright© 2020 by Turbomachinery Laboratory, Texas A&M Engineering Experiment Station

Performance curves of the trimmed trailing edge (TTE) impeller

Likewise, the normalized specific delivery work (Y/Y_{opt}) of the TTE impeller is shown in Figure 7 for different gas volume fractions. Again, the black-filled symbols and the dotted trend lines represent the results obtained by the first procedure, the empty symbols, and the dashed trend lines donate the results recorded by the second procedure, and the gray-filled symbols indicate the occurrence of pump surging. Similar to the RTE impeller, by increasing the percentage of entrained air in the mixture, the pump performance is also reduced, thereby narrowing the performance curves as the gas volume fraction is increased. Since the initial single-phase performance of the TTE impeller is lower than that of the RTE impeller, the overall performance of the TTE impeller for all various gas volume fractions is subsequently lower. Nevertheless, the TTE impeller shows here a very high gas accumulation resistance and a very robust performance with only insignificant deterioration in the specific work of the pump up to $\varepsilon = 3$ % when compared to the single-phase flow. Afterward, the performance rapidly deteriorates as for the RTE impeller due to the onset of big gas pockets on the blades. The performance degradation will be better presented in Figure 8 and further discussed.

No significant changes can be seen in the pump break-down and the cavitation regions when the two impellers are compared. However, the surging region of the TTE impeller is noticeably bigger, restricting the stable pump performance at overload conditions for $\varepsilon = 5$ % due to the strong instabilities. Further, the hysteresis effects are moderately higher, starting also from lower gas volume fractions ($\varepsilon = 3$ %), when the data of the two experimental procedures are compared.

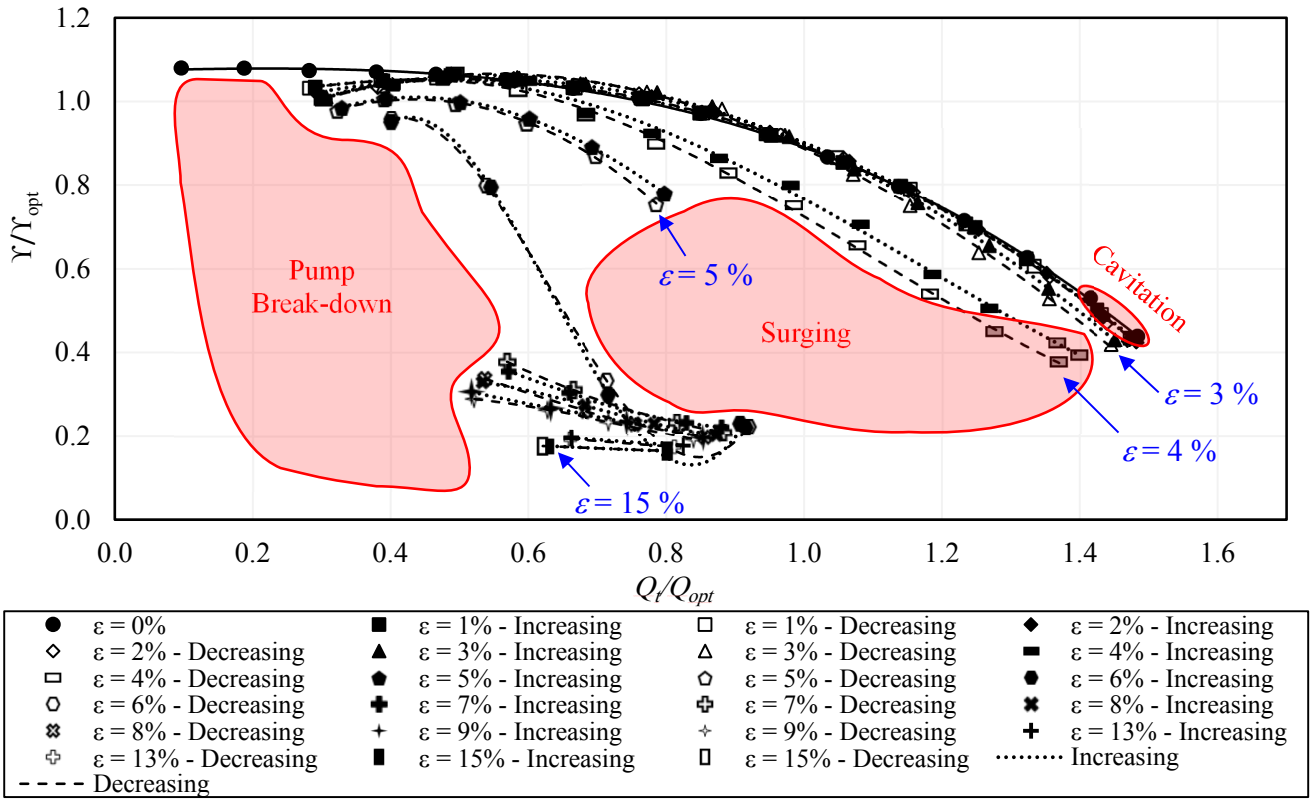

Figure 7: Normalized specific delivery work of the trimmed trailing edge (TTE) impeller recorded by the first procedure (filled symbols and dotted curves) and the second procedure (empty symbols and dashed curves).

Copyright© 2020 by Turbomachinery Laboratory, Texas A&M Engineering Experiment Station

Performance degradation

The degradation behavior of the normalized specific delivery work of the two cases is compared in Figure 8, when the gas volume fraction is increased. Concerning the RTE impeller performance shown in Figure 8a, the performance degradation is very gradually up to a gas volume fraction of 3 % for all different flow rates. However, starting from $\varepsilon = 4$ %, the pump performance sharply drops, since big pockets start to form quickly along the blades, reducing the ability of the pump to convey the mixture. Concerning the TTE impeller, although the values of the normalized specific delivery work are overall lower for single-phase flow, the performance degradation is negligible up to $\varepsilon = 3$ %, in particular for low flow rates. Nevertheless, the performance deteriorates rapidly afterward at higher gas volume fractions.

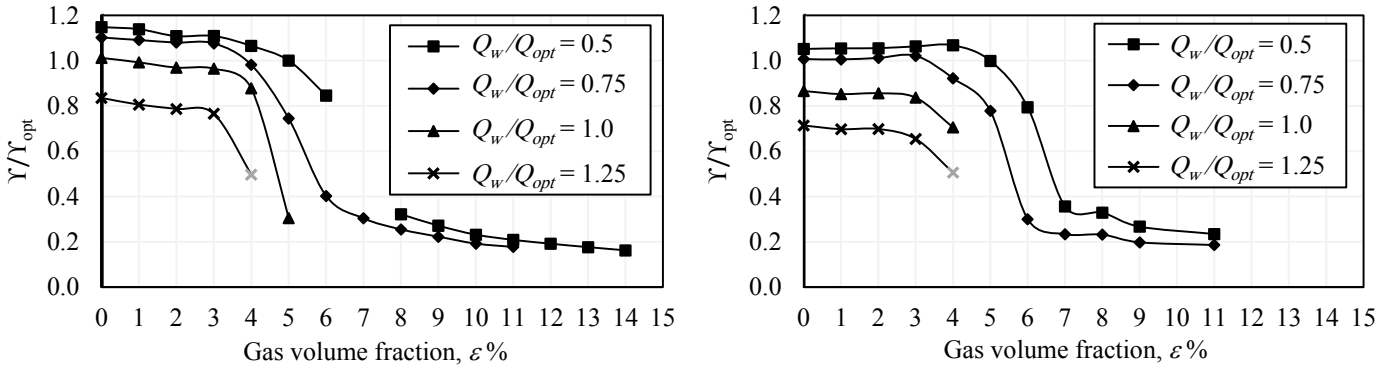

a) Round trailing edge (RTE) impeller. b) Trimmed trailing edge (TTE) impeller.

Figure 8: Degradation of the pump specific work as a function of gas volume fraction (gray symbols indicate surging conditions).

Surging and flow instabilities

Few data points could be recorded under surging conditions for both impellers. Now, the flow instabilities under surging conditions are compared to typical fluctuations due to turbulence. Figure 9 shows the standard deviation of the water flow for the two impellers. After some initial tests, it was found that 200 data points recorded at a frequency of 4 Hz are sufficient under normal conditions (no surging) to achieve a stable average of the pump parameters. While, for surging conditions, 500 data points recorded at the same frequency of 4 Hz are necessary to achieve a stable average and to track the strong, low-frequency flow variations due to surging.

Usually, the standard deviation of the water flow due to turbulence (no surging) is around 0.5 m^3/h for all cases. However, the standard deviations increase approximately to 1.5 to 3 m^3/h and to 1 m^3/h in the RTE and the TTE impellers, respectively. This change in the standard deviations indicates the occurrence of pump surging. It can be seen that surging occurs for both impellers for gas volume fractions higher than 3 % and mostly at overload conditions. Although the standard deviation of the water flow under surging conditions are weaker for the TTE impeller, it cannot be concluded that surging is generally damped in the TTE impeller since the surging region is still bigger compared to the RTE impeller and only a few data points could be recorded and compared. Overall, the RTE impeller is nonetheless recommended to ensure a limited occurrence of surging.

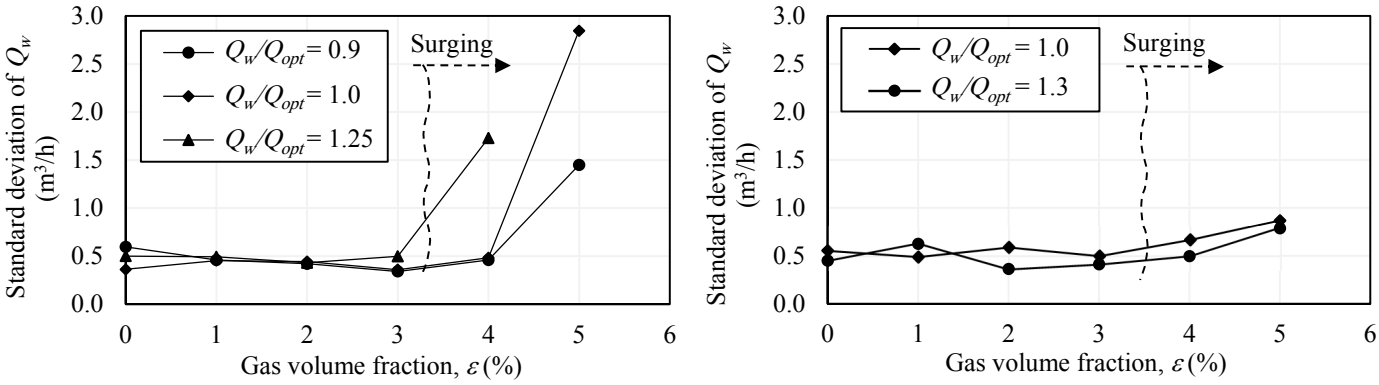

a) Round trailing edge (RTE) impeller. b) Trimmed trailing edge (TTE) impeller.

Figure 9: Representation of the flow instabilities by the standard deviation of the water flow rate.

Copyright© 2020 by Turbomachinery Laboratory, Texas A&M Engineering Experiment Station

Performance Curves for Constant Air Flow Rates

Figure 10 shows the pump performance curves obtained for constant volume flow rates of inlet air for both impellers. Again, the overall performance of the RTE impellers shown in Figure 10a is higher than that of the TTE impeller shown in Figure 10b. As shown for both cases, the reduction of the specific work is normally lower for higher flow rates of water since the gas volume fraction is correspondingly decreased. The deterioration is very limited up to Q_a = 30 L/min for both cases. Additionally, the performance curves are even overlapping for the TTE impeller for $Q_a \leq 30$ L/min, indicating very high gas accumulation resistance negligible changes compared to the single-phase performance in this range. Nevertheless, the gas accumulation resistance of the TTE impeller becomes weaker for the higher air flow rates compared to that of the RTE impeller.

The performance curves of the RTE impeller becomes slightly unstable for Q_a = 50 L/min. However, stronger instabilities can be seen for the TTE impeller at Q_a = 60 L/min. Furthermore, the working range of the pump becomes obviously narrower for the TTE impeller for $Q_a \geq 50$ L/min compared to the RTE impeller. Accordingly, the RTE impeller would be also recommended for constant air pump operation.

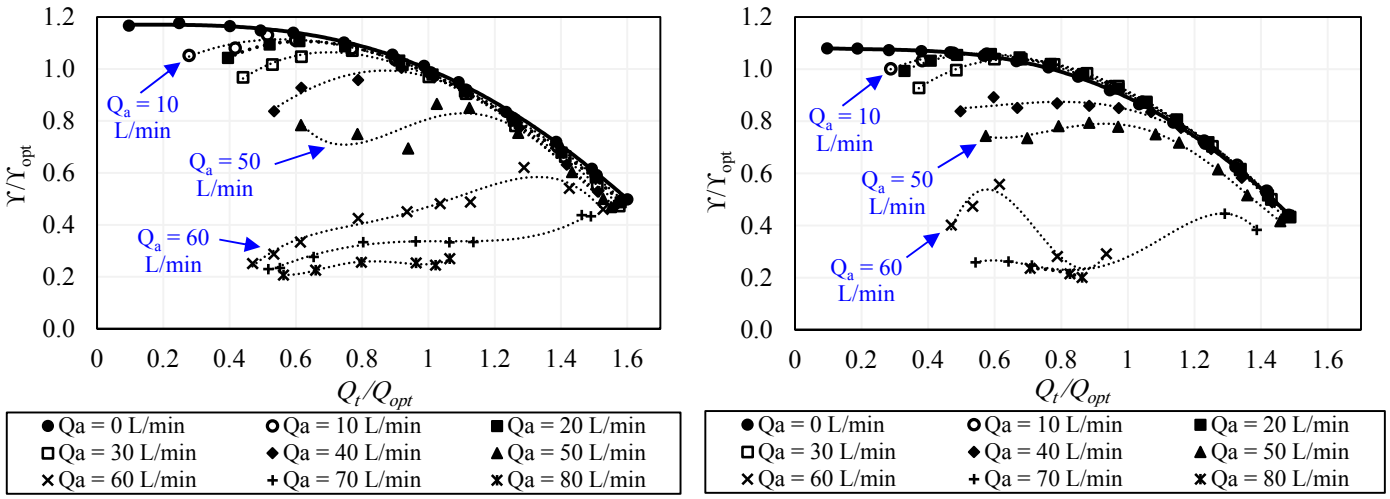

a) Round trailing edge (RTE) impeller. b) Trimmed trailing edge (TTE) impeller.

Figure 10: Performance curves for constant flow rates of inlet air.

Two-phase flow regimes

A high-speed camera with a resolution of 2016 x 2016 pixels was used to observe the flow patterns. The flow is illuminated by four high-intensity LED lamps installed periphery around the pump casing (see again Figure 1a), to make the gas-liquid interface bright and visible. The two-phase flow regimes were classified according to previous studies as listed below. Sample images of all possible flow regimes in the present work are shown in Figure 11.

1. Bubbly flow: The gas bubbles are dispersed almost everywhere in the impeller without significant interaction between them (Figure 11a).
2. Agglomerated bubbles flow: Bigger bubbles and gas pockets appear due to the coalescence of several small bubbles. This occurs near both sides of the blades with higher density on the suction side, as shown in Figure 11b.
3. Alternating pocket flow: Large (unstable) gas pockets appear mostly on the blade suction side but also and the pressure side. The pockets are characterized by strong unsteady size and location. The pockets do not appear on all blades (Figure 11c).
4. Pocket flow: Stable gas pockets appear on the suction side of all blades, with limited changes in size and location (Figure 11d).
5. Segregated flow: The gas pocket totally covers the suction side of all blades. Note that this regime could not be observed in present investigations when using semi-open impellers. It could be observed only in closed impellers.

Comparing the two cases shown in Figure 11, it can be seen that the phase interaction and the behavior of the gas accumulation are overall comparable.

Copyright© 2020 by Turbomachinery Laboratory, Texas A&M Engineering Experiment Station

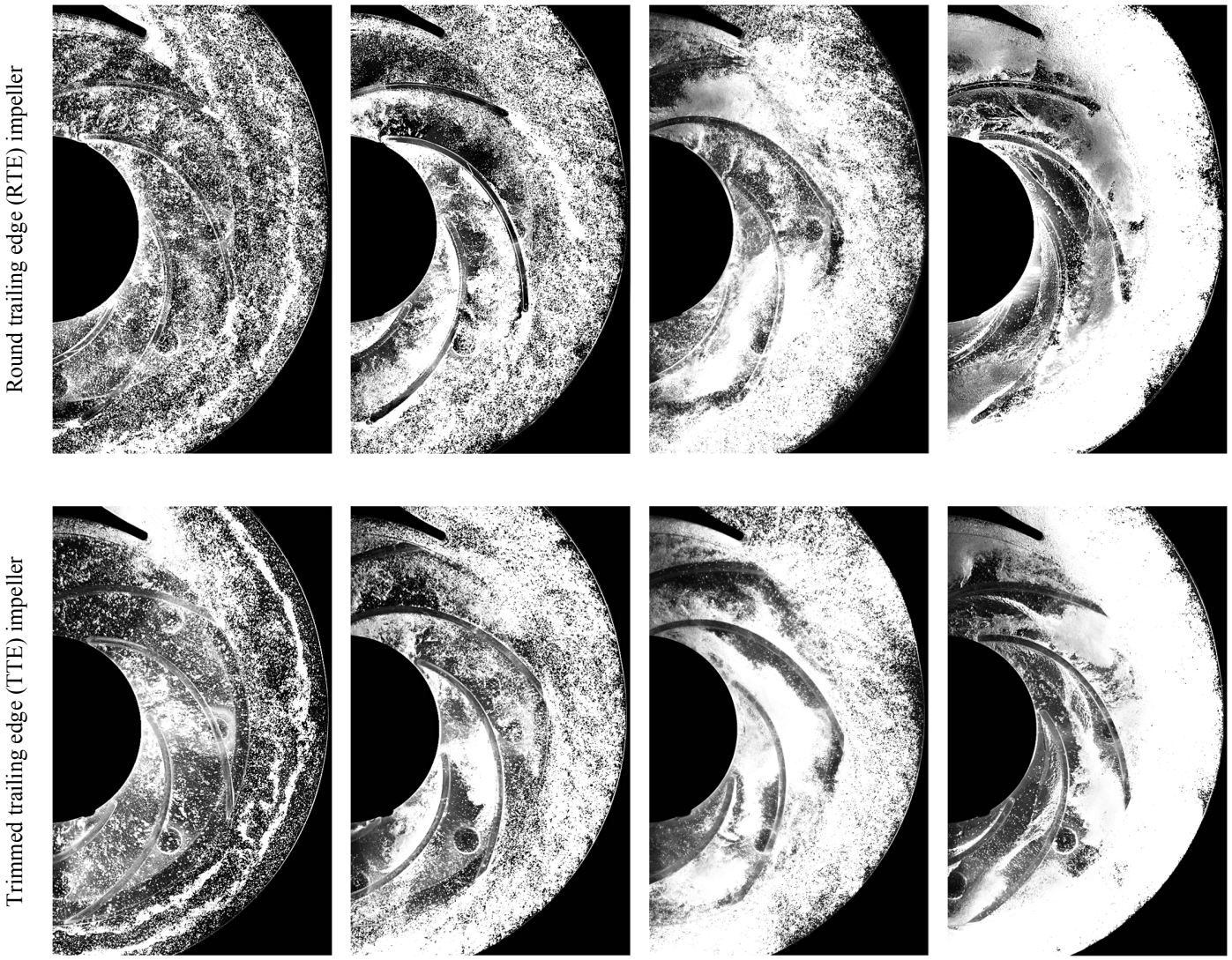

a) Bubbly (ε = 1 %, Q_t/Q_{opt} = 1.5)

b) Agglomerated bubbles (ε = 2 %, Q_t/Q_{opt} = 0.9)

c) Alternating pocket flow (ε = 2 %, Q_t/Q_{opt} = 0.25)

d) Pocket flow (ε = 6 %, Q_t/Q_{opt} = 0.8)

Figure 11: Sample images for the observed flow regimes in the pump.

Figure 12 presents detailed maps for the flow regimes and all negative phenomena associated with the performance curves of each impeller. Consequently, the behavior of the performance curves can be better understood, as a function of the existing flow regime in the impeller. Some similarities and general observations can be seen when the two maps are compared. For example, it can be seen that the bubbly flow regime occurs mainly at high flow and quite low gas volume fraction (ε < 3 %). A transition occurs to the agglomerated bubbles flow regime, when either the total flow is reduced, or the gas volume fraction is increased. Further, the dominant flow regime that occupies most of the performance curve is the pocket flow regime, which appears mostly starting from ε = 4 %. The onset of the pocket flow regime is accompanied by a remarkable drop in the performance, which is more significant at higher flows. The alternating pocket flow regime appears in part-load as well as in overload flow conditions. However, it occurs within more limited conditions for the TTE impeller. This is maybe due to the increased turbulence in this impeller which improves phase mixing. A remarkable difference between the two maps is that part of the bubbly flow regime is converted to agglomerated bubbles flow regime at overload conditions when the TTE impeller is used, due to the reduced performance. Additionally, as the gas volume fraction is increased in the pocket flow regime, the performance deterioration is worse in the TTE impeller. By comparing the two impellers further, only limited changes can be seen in the location and the size of the different flow regimes.

Copyright© 2020 by Turbomachinery Laboratory, Texas A&M Engineering Experiment Station

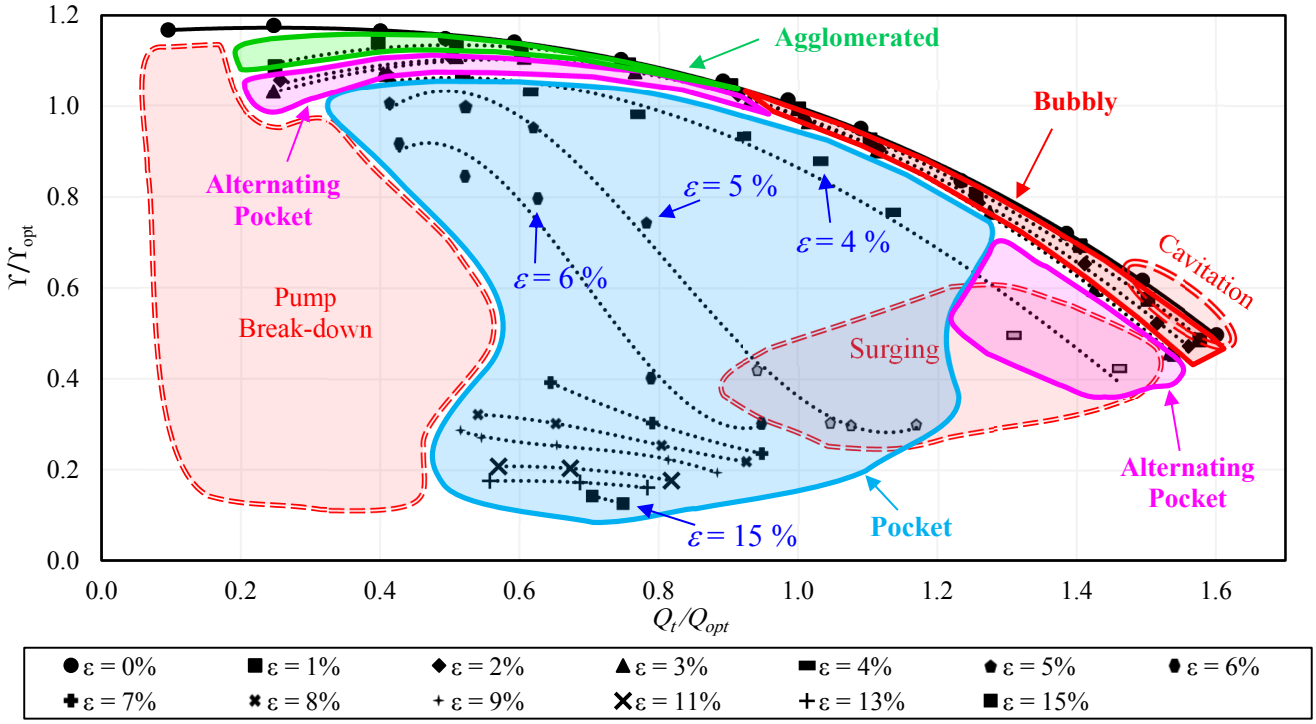

a) Round trailing edge (RTE) impeller.

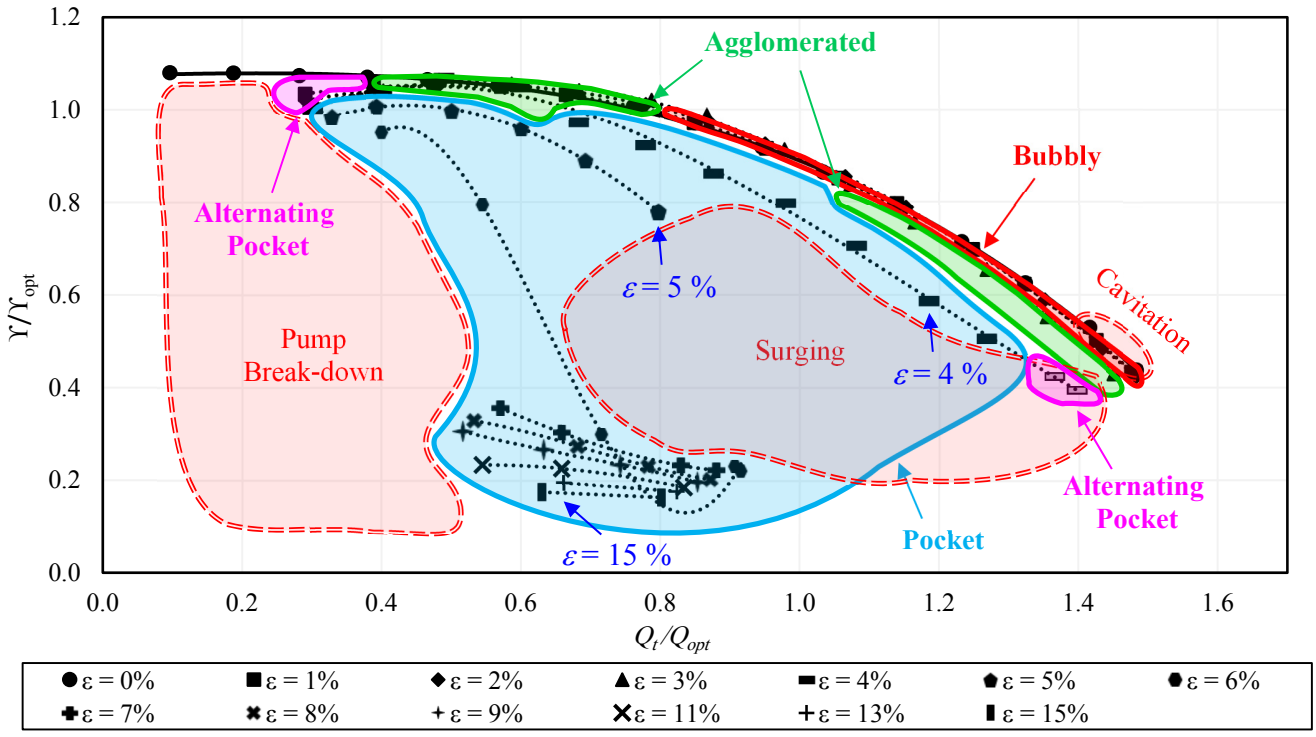

b) Trimmed trailing edge (TTE) impeller.

Figure 12: Flow regimes of the two-phase flow in the impeller.

Copyright© 2020 by Turbomachinery Laboratory, Texas A&M Engineering Experiment Station

CONCLUSIONS

The performance of a radial centrifugal pump was studied experimentally for gas/liquid two-phase flows, considering either a round trailing edge impeller (RTE) or a geometrically similar trimmed trailing edge impeller (TTE). The two impellers and the pump casing were all made of a transparent material to allow flow visualization. The two-phase flow regimes were recorded by a high-speed camera. The possible performance hysteresis was studied by applying two different experimental procedures to set the desired operating conditions, i.e. the flow rates of both phases. Additionally, to understand the performance changes between the two impellers, 3D URANS numerical single-phase simulations were performed. The main observations can be summarized as follows:

- The single-phase specific delivery work of the TTE impeller is about 7.5 to 29 % lower than that of the RTE impeller along the performance curve.
- Accordingly, for two-phase flow conditions, the overall performance and the working range of the RTE impeller is higher than for the TTE impeller.
- The numerical simulations revealed the increased flow instabilities due to the worsened blade-volute tongue interactions in the TTE impeller, compared to those of the RTE impeller.
- The simulation revealed also a noticeably bigger separation on the pump tongue for the TTE impeller compared to that of the RTE impeller at the same flow.
- Setting the desired conditions by different experimental procedures, performance hysteresis occurs in a wider range of gas volume fractions in the TTE impeller, i.e. ε = 3 – 5 %, compared to ε = 4 – 5 % in the RTE impeller.
- Although for a few measured points, the flow fluctuations of the TTE impeller were lower than those of the RTE impeller, the TTE impeller has a larger surging region and generally higher flow instabilities.
- The comparison of the two-phase regime maps described the location of each flow regime and justified the behavior of the behavior and the discontinuities in the pump behavior in both impellers.
- The two-phase regime maps confirmed that the TTE impeller is more prone to gas accumulation due to its lower performance.

According to those observations, the round trailing edge would be always preferred over the trimmed trailing edge for both single and two-phase flow performances.

NOMENCLATURE

A_1	= Suction cross-sectional area	(L^2)
A_2	= Discharge cross-sectional area	(L^2)
b_1	= Blade inlet width	(L)
b_2	= Blade outlet width	(L)
g	= Gravitational acceleration	($L\ T^{-2}$)
$\dot{m}_a$	= Mass flowrate of air	($M\ T^{-1}$)
$\dot{m}_w$	= Mass flowrate of water	($M\ T^{-1}$)
n	= Rotational speed	(T^{-1})
n_q	= Specific speed (m^3/s, m, rpm)	(T^{-1})
n_s	= Specific speed (USGPM, ft, rpm)	(T^{-1})
P_1	= Pump suction pressure	($M\ L^{-1}\ T^{-2}$)
P_2	= Pump discharge pressure	($M\ L^{-1}\ T^{-2}$)
P_{Sh}	= Shaft power	($M\ L^2\ T^{-3}$)
Q_a	= Air volume flowrate	($L^3\ T^{-1}$)
Q_{opt}	= Optimal volume flowrate	($L^3\ T^{-1}$)
Q_t	= Total volume flowrate	($L^3\ T^{-1}$)
Q_w	= Water volume flowrate	($L^3\ T^{-1}$)
R	= Gas constant of air	($L^2\ T^{-2}\ \Theta^{-1}$)
S	= Impeller tip-clearance gap	(L)
T	= Flow temperature	(Θ)
V_1	= Suction velocity	($L\ T^{-1}$)
V_2	= Discharge velocity	($L\ T^{-1}$)
z_1	= Suction elevation	(L)
z_2	= Discharge elevation	(L)
ε	= Gas volume fraction	(-)
$\dot{\mu}$	= Gas mass fraction	(-)

Copyright© 2020 by Turbomachinery Laboratory, Texas A&M Engineering Experiment Station

ρ_a	= Density of air	(M L^3)
ρ_w	= Density of water	(M L^3)
Υ	= Specific delivery work	(L^2 T^{-2})
Υ_{opt}	= Optimal specific delivery work	(L^2 T^{-2})
CFD	= Computational fluid dynamics	
CFL	= Courant–Friedrichs–Lewy number	
FS	= Accuracy in percentage of full scale	
RD	= Accuracy in percentage of reading	

REFERENCES

[1] J. Caridad, M. Asuaje, F. Kenyery, A. Tremante, O. Aguillón, Characterization of a centrifugal pump impeller under two-phase flow conditions, J. Pet. Sci. Eng. 63 (2008) 18–22. https://doi.org/10.1016/j.petrol.2008.06.005.

[2] A. Campo, E.A. Chisely, Experimental Characterization of Two-Phase Flow Centrifugal Pumps, in: ASME 2010 Power Conf., ASMEDC, 2010: pp. 803–816. https://doi.org/10.1115/POWER2010-27048.

[3] J.J. Manzano Ruiz, Experimental and theoretical study of two-phase flow in centrifugal pumps, Massachusetts Institute of Technology, 1980.

[4] A. Poullikkas, Effects of two-phase liquid-gas flow on the performance of nuclear reactor cooling pumps, Prog. Nucl. Energy. 42 (2003) 3–10. https://doi.org/10.1016/S0149-1970(03)80002-1.

[5] M. Mansour, B. Wunderlich, D. Thévenin, Effect of tip clearance gap and inducer on the transport of two-phase air-water flows by centrifugal pumps, Exp. Therm. Fluid Sci. 99 (2018) 487–509. https://doi.org/10.1016/j.expthermflusci.2018.08.018.

[6] M. Mansour, B. Wunderlich, D. Thévenin, Experimental study of two-phase air/water flow in a centrifugal pump working with a closed or a semi-open impeller, in: ASME Turbo Expo 2018 Turbomach. Tech. Conf. Expo. Pap. Number GT2018-75380, American Society of Mechanical Engineers, 2018: p. V009T27A012. https://doi.org/10.1115/GT2018-75380.

[7] Q. Jiang, Y. Heng, X. Liu, W. Zhang, G. Bois, Q. Si, A review of design considerations of centrifugal pump capability for handling inlet gas-liquid two-phase flows, Energies. 12 (2019). https://doi.org/10.3390/en12061078.

[8] J. Zhu, H. Zhu, J. Zhang, H.-Q. Zhang, An experimental study of surfactant effect on gas tolerance in electrical submersible pump (ESP), in: Vol. 7 Fluids Eng., American Society of Mechanical Engineers, 2017: p. V007T09A038. https://doi.org/10.1115/IMECE2017-70165.

[9] A. Amoresano, G. Langella, V. Niola, G. Quaremba, Advanced image analysis of two-phase flow inside a centrifugal pump, Adv. Mech. Eng. 2014 (2014) 1–11. https://doi.org/10.1155/2014/958320.

[10] Q. Si, G. Bois, Q. Jiang, W. He, A. Ali, S. Yuan, Investigation on the Handling Ability of Centrifugal Pumps under Air–Water Two-Phase Inflow: Model and Experimental Validation, Energies. 11 (2018) 3048. https://doi.org/10.3390/en11113048.

[11] D. Ni, M. Yang, B. Gao, N. Zhang, Z. Li, Numerical study on the effect of the diffuser blade trailing edge profile on flow instability in a nuclear reactor coolant pump, Nucl. Eng. Des. 322 (2017) 92–103. https://doi.org/10.1016/j.nucengdes.2017.06.042.

[12] E. Salehi, J. Gamboa, M. Prado, Experimental studies on the effect of the number of stages on the performance of an electrical submersible pump in two-phase flow conditions, in: WIT Trans. Built Environ., 2013: pp. 227–237. https://doi.org/10.2495/FSI130201.

[13] C.A. Cappellino, D.R. Roll, G. Wilson, Design considerations and application guidelines for pumping liquids with entrained gas using open impeller centrifugal pumps, in: Proc. 9th Int. Pump Users Symp., Turbomachinery Laboratories, Department of Mechanical Engineering, Texas A&M University, 1992: pp. 262–264.

[14] M. Mansour, P. Kováts, B. Wunderlich, D. Thévenin, Experimental investigations of a two-phase gas/liquid flow in a diverging horizontal channel, Exp. Therm. Fluid Sci. 93 (2018) 210–217. https://doi.org/10.1016/j.expthermflusci.2017.12.033.

[15] J. Gamboa, M. Prado, Review of electrical-submersible-pump surging correlation and models, SPE Prod. Oper. 26 (2011) 314–324. https://doi.org/10.2118/140937-PA.

[16] J. Zhu, X. Guo, F. Liang, H.Q. Zhang, Experimental study and mechanistic modeling of pressure surging in electrical submersible pump, J. Nat. Gas Sci. Eng. 45 (2017) 625–636. https://doi.org/10.1016/j.jngse.2017.06.027.

[17] W. Monte Verde, J.L. Biazussi, N.A. Sassim, A.C. Bannwart, Experimental study of gas-liquid two-phase flow patterns within centrifugal pumps impellers, Exp. Therm. Fluid Sci. 85 (2017) 37–51. https://doi.org/10.1016/j.expthermflusci.2017.02.019.

[18] P. Tillack, Förderverhalten von Kreiselpumpen bei viskosen, gasbeladenen Flüssigkeiten [Pumping behaviour of centrifugal pumps for viscous, gas-laden liquids], Technische Universität Kaiserslautern, 1998. DISS.

[19] M. Sauer, Einfluss der Zuströmung auf das Förderverhalten von Kreiselpumpen radialer Bauart bei Flüssigkeits-/Gasförderung [Influence of the inflow on the pumping behaviour of centrifugal pumps of radial design for liquid/gas pumping], Technische Universität Kaiserslautern, 2003.

[20] C. Shao, C. Li, J. Zhou, Experimental investigation of flow patterns and external performance of a centrifugal pump that transports gas-liquid two-phase mixtures, Int. J. Heat Fluid Flow. 71 (2018) 460–469.

Copyright© 2020 by Turbomachinery Laboratory, Texas A&M Engineering Experiment Station

[21] J. Zhang, S. Cai, Y. Li, H. Zhu, Y. Zhang, Visualization study of gas-liquid two-phase flow patterns inside a three-stage rotodynamic multiphase pump, Exp. Therm. Fluid Sci. 70 (2016) 125–138. https://doi.org/10.1016/j.expthermflusci.2015.08.013.
[22] K. Sekoguchi, S. Takada, Y. Kanemori, Study of air-water two-phase centrifugal pump by means of electric resistivity probe technique for void fraction measurement: 1st report, measurement of void fraction distribution in a radial flow impeller, Bull. JSME. 27 (1984) 931–938.
[23] J. Zhu, H. Zhu, J. Zhang, H.Q. Zhang, A numerical study on flow patterns inside an electrical submersible pump (ESP) and comparison with visualization experiments, J. Pet. Sci. Eng. 173 (2019) 339–350. https://doi.org/10.1016/j.petrol.2018.10.038.
[24] J. Zhu, H.-Q. Zhang, Mechanistic modeling and numerical simulation of in-situ gas void fraction inside ESP impeller, J. Nat. Gas Sci. Eng. 36 (2016) 144–154.
[25] L. Zhou, W. Shi, W. Cao, H. Yang, CFD investigation and PIV validation of flow field in a compact return diffuser under strong part-load conditions, Sci. China Technol. Sci. 58 (2015) 405–414. https://doi.org/10.1007/s11431-014-5743-6.
[26] Q. Si, G. Bois, K. Zhang, J. Yuan, Air-water two-phase flow experimental and numerical analysis in a centrifugal pump, in: 12th Eur. Conf. Turbomach. Fluid Dyn. Thermodyn. ETC 2017, 2017. https://doi.org/10.29008/etc2017-054.
[27] T. Parikh, M. Mansour, D. Thévenin, Investigations on the effect of tip clearance gap and inducer on the transport of air-water two-phase flow by centrifugal pumps, Chem. Eng. Sci. 218 (2020) 115554. https://doi.org/10.1016/j.ces.2020.115554.
[28] B. Kye, K. Park, H. Choi, M. Lee, J.-H. Kim, Flow characteristics in a volute-type centrifugal pump using large eddy simulation, Int. J. Heat Fluid Flow. 72 (2018) 52–60. https://doi.org/10.1016/j.ijheatfluidflow.2018.04.016.
[29] B. Schiavello, Two-phase flow rotodynamic pumps-experiments and design criteria, Pumps Offshore, Course. (1986).
[30] J.-W. Suh, H.-M. Yang, Y.-I. Kim, K.-Y. Lee, J.-H. Kim, W.-G. Joo, Y.-S. Choi, Multi-objective optimization of a high efficiency and suction performance for mixed-flow pump impeller, Eng. Appl. Comput. Fluid Mech. 13 (2019) 744–762. https://doi.org/10.1080/19942060.2019.1643408.
[31] R. Tao, R. Xiao, Z. Wang, Influence of blade leading-edge shape on cavitation in a centrifugal pump impeller, Energies. 11 (2018) 2588. https://doi.org/10.3390/en11102588.
[32] R. Balasubramanian, S. Bradshaw, E. Sabini, Influence of impeller leading edge profiles on cavitation and suction performance, in: Middle East Turbomach. Symp. 2013 Proceedings., Turbomachinery Laboratory, Texas A&M Engineering Experiment Station, 2013.
[33] J.F. Gülich, Centrifugal Pumps, Springer Berlin Heidelberg, 2014. https://doi.org/10.1007/978-3-642-40114-5.
[34] B. Gao, N. Zhang, Z. Li, D. Ni, M.G. Yang, Influence of the blade trailing edge profile on the performance and unsteady pressure pulsations in a low specific speed centrifugal pump, J. Fluids Eng. Trans. ASME. 138 (2016) 1–10. https://doi.org/10.1115/1.4031911.
[35] J. Keller, E. Blanco, R. Barrio, J. Parrondo, PIV measurements of the unsteady flow structures in a volute centrifugal pump at a high flow rate, Exp. Fluids. 55 (2014) 1820. https://doi.org/10.1007/s00348-014-1820-7.
[36] N. Zhang, X. Liu, B. Gao, X. Wang, B. Xia, Effects of modifying the blade trailing edge profile on unsteady pressure pulsations and flow structures in a centrifugal pump, Int. J. Heat Fluid Flow. 75 (2019) 227–238. https://doi.org/10.1016/j.ijheatfluidflow.2019.01.009.
[37] B. Li, X. Li, X. Jia, F. Chen, H. Fang, The role of blade sinusoidal tubercle trailing edge in a centrifugal pump with low specific speed, Processes. 7 (2019) 625. https://doi.org/10.3390/pr7090625.
[38] H.A. Warda, S. Haddara, I.G. Adam, Blade trailing edge profile effect on low specific speed centrifugal pump performance, in: 11th Int. Conf. Role Eng. Towar. A Better Environ. Bridg. Gap Acad. Gov. Ind. Alexandria, Egypt, 2017.
[39] F.R. Menter, Two-equation eddy-viscosity turbulence models for engineering applications, AIAA J. 32 (1994) 1598–1605. https://doi.org/10.2514/3.12149.
[40] W. Zhang, Z. Yu, B. Zhu, Numerical study of pressure fluctuation in a gas-liquid two-phase mixed-flow pump, Energies. 10 (2017) 634. https://doi.org/10.3390/en10050634.
[41] X. Li, S. Yuan, Z. Pan, Y. Li, W. Liu, Dynamic characteristics of rotating stall in mixed flow pump, J. Appl. Math. 2013 (2013).
[42] T. Müller, P. Limbach, R. Skoda, Numerical 3D RANS simulation of gas-liquid flow in a centrifugal pump with an Euler-Euler two-phase model and a dispersed phase distribution, in: Proc. 11th Eur. Conf. Turbomachinery, Fuild Dyn. Thermodyn. Madrid, Spain, 2015: pp. 23–25.
[43] T. Müller, P. Limbach, R. Skoda, Influence of Geometry Simplifications and Numerical Parameters in 3D URANS Liquid-Gas Flow Simulations of a Radial Pump with an Eulerian Mono-Dispersed Two-Phase Model, in: Proc. 16th Int. Symp. Transp. Phenom. Dyn. Rotating Mach. ISROMAC 2016, Honolulu, Hawai, 2016.
[44] M. Hundshagen, M. Mansour, D. Thévenin, R. Skoda, Numerical investigation of Two-Phase air-water flow in a centrifugal pump with closed or semi-open impeller, in: 13 Th Eur. Conf. Turbomach. Fluid Dyn. Thermodyn., European Turbomachinery Society, 2019.
[45] Siemens PLM Software Inc., STAR-CCM+ Version 13.02.013 User Guide, Plano, TX, USA, 2018.
[46] J. Jeong, F. Hussain, On the identification of a vortex, J. Fluid Mech. 285 (1995) 69–94.
[47] M. MurakamiI, K. Minemura, M. Takimoto, Effects of entrained air on the performance of centrifugal pumps under cavitating conditions, Bull. JSME. 23 (1980) 1435–1442. https://doi.org/10.1299/jsme1958.23.1435.

Copyright© 2020 by Turbomachinery Laboratory, Texas A&M Engineering Experiment Station

[48] A.R. Budris, P.A. Mayleben, Effects of entrained air, NPSH margin, and suction piping on cavitation in centrifugal pumps, in: Proc. 15th Int. Pump Users Symp., Texas A&M University. Turbomachinery Laboratories, 1998. https://doi.org/10.21423/R1339N.

ACKNOWLEDGMENTS

The authors gratefully acknowledge the financial support of this project by the Verband Deutscher Maschinen- und Anlagenbau e.V. (VDMA), as part of a collaboration with Professor R. Skoda from Ruhr University in Bochum. The Ph.D. work of Dr. Mansour was partially supported by a scholarship from the Egyptian government.

Copyright© 2020 by Turbomachinery Laboratory, Texas A&M Engineering Experiment Station